Coupled Ocean-Acoustic prediction of transmission loss in a continental shelfbreak region: predictive skill, uncertainty quantification and dynamical sensitivities

Pierre F.J. Lermusiaux and Jinshan Xu

This work was supported by the U.S. Office of Naval Research under the QPE grants N00014-07-1-0241 and N00014-08-1-0586 to MIT.

P.F.J. Lermusiaux (email: pierrel@mit.edu) and J. Xu (email: jinshan@mit.edu) are with the Department of Mechanical Engineering, Massachusetts Institute of Technology, Cambridge, MA, 02139 USA (webpage: http://mseas.mit.edu/)

Report Documentation Page

Form Approved
OMB No. 0704-0188

1. REPORT DATE	2. REPORT TYPE	3. DATES COVERED
2010		**00-00-2010 to 00-00-2010**

4. TITLE AND SUBTITLE	5a. CONTRACT NUMBER
Coupled Ocean-Acoustic prediction of transmission loss in a continental shelfbreak region: predictive skill, uncertainty quantification and dynamical sensitivities	5b. GRANT NUMBER
	5c. PROGRAM ELEMENT NUMBER
6. AUTHOR(S)	5d. PROJECT NUMBER
	5e. TASK NUMBER
	5f. WORK UNIT NUMBER
7. PERFORMING ORGANIZATION NAME(S) AND ADDRESS(ES) **Massachusetts Institute of Technology,Department of Mechanical Engineering,Cambridge,MA,02139**	8. PERFORMING ORGANIZATION REPORT NUMBER
9. SPONSORING/MONITORING AGENCY NAME(S) AND ADDRESS(ES)	10. SPONSOR/MONITOR'S ACRONYM(S)
	11. SPONSOR/MONITOR'S REPORT NUMBER(S)

12. DISTRIBUTION/AVAILABILITY STATEMENT
Approved for public release; distribution unlimited

13. SUPPLEMENTARY NOTES
IEEE Transactions, Journal of Oceanic Engineering. Submitted

14. ABSTRACT
see report

15. SUBJECT TERMS

16. SECURITY CLASSIFICATION OF:			17. LIMITATION OF ABSTRACT	18. NUMBER OF PAGES	19a. NAME OF RESPONSIBLE PERSON
a. REPORT	b. ABSTRACT	c. THIS PAGE			
unclassified	**unclassified**	**unclassified**	**Same as Report (SAR)**	**38**	

Abstract

In this study, we explain and quantify the dynamical causes of striking differences in the acoustic transmission data collected on the shelf and shelfbreak in the north-eastern Taiwan region within the context of the Quantifying, Predicting and Exploiting (QPE) uncertainty 2008 Pilot Experiment. To do so, we employ our own coupled oceanographic(4D)-acoustic(Nx2D) modeling systems with ocean data assimilation and a best-fit depth-dependent geo-acoustic model. For the first time, predictions are compared to the measured acoustic data, showing skill. We also study the sensitivity of our results to uncertainties in several factors, including geo-acoustic parameters, bottom layer thickness, bathymetry and ocean conditions. Our simulations first reveal that the lack of signal received on the shelfbreak is due to a dramatic 20 dB increase in transmission loss (TL) caused by bottom trapping of sound energy during up-slope transmissions over the complex and deeper bathymetry. Sensitivity studies on sediment properties show larger but isotropic TL variations on the shelf and smaller but more anisotropic TL variations over the shelfbreak. Diverse thicknesses of sediments lead to only limited effects on the TL. The small bathymetric data uncertainty are modeled and also shown to lead to small TL variations. We discover that the initial transport conditions in the Taiwan Strait can affect acoustic transmissions downstream more than 100 km away, especially above shelfbreak. Simulations also reveal internal tides and quantify their spatial and temporal effects on the the ocean and acoustic fields. One type of waves found are shelfbreak internal tides propagating up-slope with wavelengths around 40-to-80 km and vertical displacement of isotherms of 10-to-20 m. These waves lead to variations of broadband TL estimates over 5-6 km range that are more isotropic and on bearing-average larger (up to 5 dB) on the shelf than on the complex shelfbreak where the TL varies rapidly with bearing angles.

Index Terms

Data assimilation, underwater acoustics, shelf and shelfbreak sound propagation, uncertainty quantification, interdisciplinary modeling

I. Introduction and Motivation

As one of the major application of underwater acoustics, sonar performance prediction requires modeling the acoustic field evolution. In the littoral ocean environment, the time and space scales relevant for such predictions can be minutes to a week and hundreds of meters to tens of kilometers. The parameters include the four-dimensional ocean and seabed fields. They are complex to predict and can have significant uncertainties [1], [2]. Methods and systems that forecasts the ocean, the seabed and the acoustics in an integrated fashion have only been developed and utilized recently [3]–[6]. Acoustic data were previously not available for evaluations of such

systems. An objective of the present investigation is to compare predictions of such coupled systems to in situ acoustic data. Even though important, such comparisons had not been done before.

Our approach is based on coupling data-assimilative environmental and acoustic propagation models with ensemble simulations, as developed by [4], [5], [7], [8]. This approach was applied with adaptive sampling and onboard routing within the Focused Acoustic Forecasting-05 (FAF05) excercise [9]. During the PN07 exercise in Dabob Bay, acoustic transmission loss fields were also coupled to data-assimilative ocean fields by Xu et al. [10] so as to characterize impacts of wind forcing and tidal forcing on acoustic fields and performance. Within the scope of Battlespace Preparation 2007 (BP07), Lam et al. [11] coupled acoustic and ocean models at sea in real-time, Rixen et al. [12] utilized super-ensemble prediction techniques for acoustic inversion and tomography, Carriére et al. [13] investigated full-field tomography and tracking, and Martins and Jesus [14] studied acoustic prediction as a Bayesian estimation problem. The New England Shelbfreak front region e.g. [15]–[17] and the shallow Asian Seas e.g. [18]–[22] have also seen major ocean and acoustic studies with coordinated sampling. The results of all these efforts show that ocean variability can considerably influence acoustic propagation properties both in time and in space. Acoustic propagation in shallow water is also known to be strongly affected by multiple seabed interactions and bathymetry effects [23]. In continental shelf break regions, the seabed and bathymetry are especially complex and not well known. Uncertainties in geoacoustic modeling usually come from the imperfect knowledge of the true thicknesses and properties of the sediment and rock layers in the sea floor. Studying and quantifying the sensitivity of our coupled predictions to key ocean and geoacoustic uncertainties is another objective of our present effort.

Our investigations are part of the Quantifying, Predicting, and Exploiting Uncertainty (QPE) initiative which aims to integrate probabilistic performance prediction, coupled ocean-acoustic modeling, multidisciplinary data assimilation and autonomous ocean platforms to improve performance prediction and reduce detection uncertainties. Our focus is on the QPE 2008 pilot exercise [24] carried out on the continental shelf and slope of northeast Taiwan in September, 2008. The main goals of this 2008 exercise were to test systems and methodologies to measure and forecast the baseline regional ocean variabilities and uncertainties, as well as their impacts on low-frequency (100 to 1000Hz) acoustic propagation conditions. Two main locations were chosen for the exercise, one on the continental shelf and the other on the shelfbreak. Interestingly,

the transmission loss over ranges of 5 to 6 km over circular areas in these two regions were observed to be very different. This occurred even though the two circular areas overlapped in space. For example, no signal was obtained when the source was over the deeper water on the shelfbreak, and the measured mean and variability of the transmission loss differed greatly in the two regions. In real-time and after the experiment, the community could not explain the causes of these differences. To understand and quantify these observed behaviors, both acoustic and environmental dynamical modeling are required.

In the present study, we utilize coupled oceanographic(4D) and acoustic(Nx2D) fullfield simulations to explain and quantify the mean and dynamic variability of mid-frequency sound transmission losses observed during the QPE 2008 Pilot experiment northeast of Taiwan. To do so, coupled model estimates are for the first time compared to the underwater acoustic observations available. We also investigate the sensitivity of the TL estimation to uncertainties in geo-acoustic parameters, bathymetry, sediment layer thicknesses and initial transports in the Taiwan Strait as well as to background sound speed variability involving tidal effects.

In what follows, we first outline the QPE 2008 Pilot experiment and the corresponding observations and coupled modeling systems (Sect. II). In Sect. III, the transmission loss data and its variability with respect to positions and bearing angles are compared with our coupled oceanographic-acoustic modeling predictions. The uncertainties in the TL estimates due to various factors are also modeled and quantified, and the sensitivity of these TL estimates to ocean variability is computed and studied. The summary and conclusions are in Sect. IV.

II. Real-time Experiment, In-situ Observations and Coupled Modeling Systems

The QPE 2008 Pilot Cruise was carried out on the continental shelf and slope of northeast Taiwan (Figure 1). Most of the acoustic propagation experiments were conducted inside the rectangular boxed region just north of ($25.5°$N,$122.5°$E). Our regional dynamics and modeling focus was the continental shelf and slope northeast of Taiwan, and especially the Cold Dome (e.g. [25]), its dynamics, variabilities and uncertainties, as well as impacts of this environment on low/mid-frequency (100 to 1000 Hz) acoustic propagation. In the region, a large number of ocean processes can occur simultaneously, very energetically and on multiple scales [24], [26]–[28]. The ocean observations, the coupled ocean-acoustic modeling systems used for real-time predictions and the acoustic observations are described next.

A. Ocean Observations

The Pilot Experiment involved three separate cruises to collect ocean environmental data (see Figure 1(a) for CTD stations positions). The solid dots are for the OR1 cruises: Leg 1 was operated between the Ilan Ridge and the Main Study Area during September 2-4 while Leg 2 was in the Main Study Area from September 6-11. The stars and circles indicate the stations that the vessels operated during August 22-27 (respectively, the OR2 northeast of Taiwan and the OR3 in the Taiwan Strait). As soon as available, these CTD measurements, as well as other measurements were assimilated in our simulations.

B. Real-time Modeling Systems and Coupled Predictions

In real-time, we carried out sustained coupled-oceanographic(4D)-acoustic(Nx2D) fullfield simulations for a 7-day long period [26], each day selecting a subset of these simulations as the acoustic-ocean forecast for the next two days. Our simulations utilized the MIT Multidisciplinary Simulation, Estimation and Assimilation System (MSEAS). This system is used for realistic simulations and real-time forecasts in several regions of the world's ocean. For the ocean dynamics, it employs a new free-surface and two-way nested primitive-equation code [29] (a significant upgrade of the rigid-lid Harvard primitive-equation model [30], [31]). The MSEAS system also involves a coastal objective analysis scheme based on fast-marching methods [32]; an Optimal Interpolation scheme and Error Subspace Statistical Estimation system (ESSE, [33]–[36]) for data assimilation, optimization and adaptive sampling; new schemes for uncertainty predictions based on dynamically-orthogonal equations [37]; multiple biological models [38]; and, several acoustic models.

The QPE ocean simulations were forced with barotropic tidal flows [39] at open ocean boundaries and with a combination of COAMPS (wind stress) and NOGAPS (heat-flux, E-P) atmospheric forcing at the air-sea interface. Fields were initialized with the OR2 and OR3 CTD data merged with a summer climatology created using June-August profiles and the HydroBase2 software [40]. The bathymetry used was the NCOR bathymetry [41]. The OR1 CTD and the Seasoar data were assimilated when available. During the preparation of the exercise, we found that the net transport between Taiwan and mainland China can have a significant influence on the formation and strength of the cold dome, especially just north of Taiwan. To account for the corresponding uncertainty in real-time, 2-3 different initial transport cases were utilized for each ocean forecast (of course, boundary conditions vary in time with a radiation condition [42], but

the radiation condition is applied to the departure from this initial estimate [43] which remains fixed). The skill of the ocean predictions obtained from each of these different initial boundary condition cases were computed in real-time by daily comparisons to the available in situ data and SST [44].

The ocean forecasts and their uncertainties were used as inputs to the acoustic simulations. The bathymetry data were provided by the Center for Coastal and Ocean Mapping with up to 100 m resolution in the main study region [45]. Acoustic simulations were performed with the Coupled SACLANTCEN normal mode propagation loss model (C-SNAP) [46] using the sound-speed fields of MSEAS as parameters. In real-time, transmission loss forecasts were provided along five 20 km-long acoustic propagation paths which had been pre-selected to explore the variability in this region. Real-time results are presented in [26]. Specifics on our acoustic modeling and results are provided in Section III. As a whole, the QPE scientific team successfully resolved the Cold Dome, preformed data transfer in real time and forecasted oceanographic and acoustic propagation conditions daily, including uncertainties in ocean fields due to uncertainty in the Taiwan Strait transport.

C. Acoustic Propagation Observations

The acoustic propagation experiments were conducted during the leg 2 of the Pilot Cruise on OR1. The OMAS vehicles were utilized as sound sources. The receivers included standard US Navy sonobouys and the NTU vertical line array (VLA). Four OMAS events were carried out, two on the shelf along relatively constant headings and depths and two in circular tracks around the shelfbreak region.

The first two events conducted on the shelf occurred at approximately 110 m to 130 m depth. The OMAS moved at a speed of 5 knots. Our numerical modeling results of these first two events were compared and fitted to the transmission loss observations at different ranges, providing insights on the values of the geoacoustic model parameters. Fits were good but results are not shown here.

The other two acoustic events were the two circular OMAS runs: Event A and B, as shown in Fig. 1(b). The northern and southern circles are the nominal Event A and B tracks, respectively. The programmed radius of Event A was set to 5 km and that of Event B to 6 km. The OMAS vehicles and the sonobuoys were set to run at 61 m in depth. The northern circle was centered at approximately 110 m in depth, and covered a relatively flat, slightly sloping bottom. The southern

circle was positioned over the steeply breaking shelf. Fig. ure 2(a) presents TL measurements collected from the two runs: the blue curve denotes the 1100 Hz TL data for Event A, the red curve is the 900 Hz TL data for Event B. Note the TL data here is the peak of the matched filer output and small linear range corrections are applied to obtain the TL estimation at the range of 6 km. The TL of Event A varies somewhat with the bearing angle, showing an increased TL in the north-eastern direction. Interestingly, during Event B (southern circle positioned over the shelfbreak), no signal was observed when the OMAS source was in the deeper waters. In addition, considering the arcs over the shelf only, the mean of the TL data was 2-5 dB larger for Event B (shelfbreak run) than for the arc of Event A (shelf run). The goals of our modeling are to explain and quantify such observations, and to investigate the variation of the TL estimates due to uncertainties in the sediments, bathymetry, and ocean water column variation.

III. RESULTS

Our simulations start with the range dependent ocean sound speed fields provided by the forecasts of our MIT MSEAS system for the period of September 1-12, 2008 (Section II-B). Acoustic TL fields were computed using C-SNAP in 180 bearing directions (2-degree resolution) for both Events A and B, at frequencies of 1100 Hz and 900 Hz, respectively. In these Nx2D computations, the two simulated OMAS circles were centered at (25°N 39.8' 122°E 35.76') and (25°N 44.55' 122°E 33.90'), with radius of 6 km, respectively. These locations are mean estimates of the positions of the slightly moving receivers' tracks [24]. The sources and receivers were set at 61 m depth below the sea surface to fit the sea configuration. Transmission losses were computed at positions that were $\pm$ 600 m in range and ± 5 m around the depth of the receiver. The average predicted TL within these horizontal and depth ranges was then set to be our TL estimate because it is a good approximation [47] to the 10 percent bandwidth of frequency averaging that occurred in the real in situ broadband propagation. All of the Nx2D TL estimates that we show in this manuscript are broadband estimates, but they are often simply referred to as TL. The first results of our coupled ocean-acoustic simulations are illustrated in Figure 2(b), with Event A at 12:00, September 8, 2008, and Event B at 15:00, September 8, 2008 (all UTC times). Shown are our broadband TL estimates for the time and location of the two events, for all bearing angles. If we consider only the range of bearing angles for which a signal was received at sea from the OMAS runs, our mean TL estimates for Event A and Event B are about 77-81 dB and 79-85 dB, respectively. These predicted numbers are in good

agreement with the mean data received, as illustrated on Fig. 2(a). In fact, this is the first time that coupled ocean-acoustic predictions are validated using *in situ* acoustic data. The measured and predicted mean TL are within 1 to 3dB, which is within the uncertainties of our coupled acoustic-ocean simulations (Sect. III). In addition to the mean values, spatial patterns are also captured. For example, for Event A, one notes the increased TL in the north-eastern direction (225^o to 45^o), in accord with the data (Fig. 2(a)): this is linked to ocean variability as shown in Sect. III-D. For Event B, our simulated mean TL on the shelf is also lower by 2-5 dB than that of Event A along the same angles, as was observed: this result is linked to seabed properties (Sect. III-A).

The bathymetry data (see Fig.1(c)) along bearing angles of 120 to 230^o shows depth variations from 150 m to more than 300 m. In our coupled modeling results, this leads to a mean TL estimate for Event B that is higher by 15-20 dB than the mean TL of Event A along the same angles (Figure 2(b)). We expect that this explains why there was no reception during the Event B run when the OMAS went over this deeper shelfbreak region. At these angles, this leads to an up-slope transmission which causes extensive transmission loss. However, since the ocean, seabed and bathymetry are all uncertain, it is also possible that some water column, seabed or bathymetric features were the causes, or were at least in part responsible, of this behavior. To study and quantify these possibilities, we investigate next the sensitivity of our broadband TL estimates to uncertainties in geo-acoustic parameters (sediment thickness and sediment types), bathymetry, and variability of the ocean sound speed fields (Taiwan strait transport and tidal dynamics). We also quantify the effects of these uncertainties on the mean TL estimates. For each uncertainty factor, we compute the standard deviations of our TL estimates (assuming all other factors constant and perfectly known). Of course, these standard deviations differ from the standard deviations of the TL measured at sea. This is because the standard deviations of the measured TL correspond only to variations in the ocean and in the positions/bearing during the given OMAS circle run (assuming the bathy and seabed properties are fixed during that time).

A. TL sensitivities to uncertainties in the Geoacoustic model - sediment types and thicknesses

Uncertain factors in the geoacoustic model that lead to uncertainties in the TL estimates include the thicknesses and properties of the sediment and rock layers in the sea floor. At higher sound frequencies, the first few to tens of meters of sediments matter most. At lower frequencies, the whole sediment column and underlying rocks often matter. A challenge for precise modeling of

sound propagation in this region is the lack of knowledge of the geo-acoustic parameters. For our frequencies (900 and 1110 Hz), we evaluated and compared more than thirty sediment models. Here we only report a few of them including the properties of sand, muddy-sand, silty-clay and hybrid models in Tables I and II. Specifically, Table I gives three sediment types including an additional half-space basement, while Table II gives our best-fit so far, an hybrid and depth-dependent model. For each sediment, note that the first line corresponds to the optimum values we obtained using the hybrid model, while the second line indicates the deviation ranges of the parameter values that we tested on. The first three sediments followed Hamilton's models [48], [49]. The hybrid depth-dependent models were the best-fit results of our multiple comparisons to data aiming to optimize parameters (three sediment types and two transition depths) and of interactions with Heaney, Holland and Chen (personal communications). A similar hybrid model was also obtained by Heaney [50].

In Figure 3, we illustrate how sediment layers affect our TL estimates for both Events A and B, showing the results for four of the models we evaluated (see Tables I and II). The sediment thickness is set to 20 m in all cases. We find that the four models have different impacts on the shelf and shelfbreak.

For Event A on the shelf, the four sediments lead to distributions of TL variation with bearing angles that are very similar. The sediment types shown lead to overall isotropic TL differences of 5 to 15 dB in all directions. The average standard deviation is 9.55 dB.

For Event B on the shelfbreak, the average standard deviation is smaller, 5.81 dB, than for Event A. The shapes of the four TL estimates are still similar, but a bit less than for Event A. The TL deviations due to different sediments are estimated to be lesser along the shelfbreak (e.g. 5 dB or less) but a bit larger towards the shelf (e.g. about 7-8 dB along 330^o) and for bearing angles of 120^o to 240^o which is over the deeper bathymetry region. In fact, the steepest bathymetries lead to a very localized amplification of TL uncertainties due to sediment uncertainties: TL deviations are maximum (30 dB) along the bearing angle of 180^o. Nonetheless, all TL fields of Event B for bearing angles of 120^o to 240^o clearly show a much higher TL than in Event A (on average, by about 20 db), as was measured at sea (see Fig. 2(a)). This implies that the sediment properties cannot alone explain the observed higher loss.

We also investigated the effects that uncertainties in the thicknesses of sediment layers have on our TL estimates. The results (plots not shown here) indicate that variations of 5 to 25 m in the sediment thicknesses have some limited effects only on the up-slope transmissions for

the circle runs of both Event A (less than 2 dB uncertainty) and Event B (less than 2-3 dB uncertainty, excepted in the deeper region where it reaches 3-6 dB).

An important result of these sensitivity studies to uncertainties in both sediment types and thicknesses is that neither of them can alone explain the lack of transmission for Event B when the OMAS source moved over the deeper shelfbreak. A combination of both uncertainties (not shown) still does not change this conclusion. Therefore, the bathymetry itself is found responsible for the lack of transmission. A second result is that although the full geo-acoustic inversion has not yet been completed for this site, our simple optimized hybrid sediment model and sediment thickness (20 m) with our 4D simulations of the ocean sound speed lead to predicted estimates of the broadband TL that are in good agreement with the measurements (see Fig. 2(b)).

B. TL sensitivities to uncertainties in bathymetry

Since we found that bathymetry is likely responsible for causing the loss of acoustic reception in Event B over the shelfbreak, we estimated the TL variations due to uncertainties in the bathymetry. By comparing bathymetries of different resolutions and different origins, we obtained a general characteristic: errors in bathymetry are a function of the depth and slope. Therefore, we derived a simple model of the probability density of the baythmetry around its best estimate (100m resolution). This model consists of a zero mean Gaussian noise with variance a function of the slope and depth, i.e.,

$$D(r;\omega) = D(r)[1 + \sigma(r) \cdot \omega], \tag{1}$$

where $D(r;\omega)$ is a stochastic process, Ω is the sample space containing the set of elementary events $\omega \in \Omega \sim N(0,1)$, r is range and $\sigma(r) = \epsilon \cdot \hat{S}(r)$ where the normalized slope $\hat{S}(r) \subseteq [0\ 1]$. The simulation results with different realizations of this bathymetric uncertainty model are shown in Figure 4. Each TL circular curve corresponds to a bathymetric noise with different percentages of local depth and slope.

As a whole, for these levels of bathymetric uncertainties, we find that the uncertainties of our TL estimates are proportional to uncertainties in the bathymetry. Another result is that the general shape of the TL circular curves with bearing angles remains as obtained before. Therefore, bathymetric uncertainties cannot explain the observed increase in TL over the deeper ocean region. Again, bathymetry itself provides the explanation.

C. TL sensitivities to uncertainties in the ocean water column

In the following, we analyze effects of uncertainties in the mean water column on our acoustic transmission loss predictions. We focus on uncertainties in the transport through the Taiwan Strait (ocean between mainland China and Taiwan, e.g. [51]). Even though the operational acoustic area is more than 100 km away northeast of the Taiwan Straits centerline, we had discovered (see Sect. II-B) that the strength of the Straits transport could have a significant influence on the Cold Dome region, especially just north of Taiwan [26]. If the initial Taiwan Strait transport was northward and of the order of 1Sv or more, our simulations showed that the Kuroshio had limited intrusion over the shelfbreak northeast of Taiwan and the Cold Dome did not really form. However, if the initial Taiwan Strait transport was weaker or southward, we found that deeper and cooler Kuroshio waters upwelled on the shelf and the Cold Dome could form, the strength of this formation being a function of the transport. For the acoustics in the operational area northeast of Taiwan (see Fig.1), these different ocean forcing change the mean sound speed field. They can thus have significant impacts on the TL estimates.

In real-time, we considered three different initial transport conditions through the Taiwan Strait: an initial transport of 1 Sv northward, of 1 Sv southward, and of 0 Sv. Figure 5 shows sound speed fields in the QPE-Pilot experiment region at 30 m, 60 m and 90 m depth (lines 1, 2 and 3 on Fig. 5, respectively) with different initial transport conditions through the Taiwan Strait (columns 1, 2 and 3 on Fig. 5, respectively). The main acoustic research area is denoted by a white rectangle frame. The differences of sound speed at the depth of 30 m, and 60 m depth are easily noticeable, but not as apparent at the depth of 90 m in part because the range of sound-speeds present in the region is larger at this depth.

Figure 6 illustrates our Nx2D acoustic simulations for Events A and B, using the three different sound speed backgrounds illustrated by the columns of Fig. 5. The geo-acoustic model in all cases was the hybrid depth-dependent model with a 20-m thickness of sediment layer (see Sect. III-A). The three 4D sound speed fields were predicted by our MSEAS ocean forecast system: each correspond to a different initial transport condition between Taiwan and mainland China (± 1 Sv and 0 Sv). The prediction skill for each of these initial conditions was computed in real-time daily, based on comparisons with the available in situ data and SST [44] for that day. On September 8, 2008, the 1 Sv South initial transport condition was chosen as the best ocean forecast. We find that the three ocean fields cause different effects on the acoustic transmissions of Events A and B. On Sep 8th (the day when Events were run at sea), the uncertainty in the

ocean state due to the uncertainty in the initial conditions of the Taiwan Strait transport has more impacts on our broadband TL estimates for the shelf break Event B than for the shelf Event A. For the shelf Event A, our estimated TL variations along the different bearing angles reached about 1 to 3 dB, with a bearing-averaged standard deviation of 0.58dB. However, for the shelf break Event B, our TL estimates varied almost evenly in all directions up to about 2 to 5 dB, with a bearing-averaged standard deviation of 1.21dB.

In conclusion, these results first indicate that uncertainties in the Taiwan Strait transport lead to broadband TL uncertainties that are smaller on the shelf than on the shelfbreak. This is because the shelfbreak ocean dynamics is more sensitive to this transport than the shelf dynamics. Another result is that the shape of our broadband TL curve does not vary much with these different ocean forecasts: it is mainly the mean TL which is affected. This indicates that the lack of signal received for Event B when the OMAS passed over the deeper shelfbreak region is not due to these ocean uncertainties (themselves due to the uncertain initial conditions of the Taiwan Strait transport). The bathymetry remains the explanation.

D. TL sensitivities to tidal dynamics in the ocean water column

We now examine the variations of the transmission loss field due to variability in the ocean, specifically tidal effects. We focus on internal tidal variability because our data-assimilative simulations revealed that semi-diurnal frequencies in the ocean interior led to significant variations in the sound energy transmitted. First, we characterize this ocean variability, then we study its impacts on the broadband sound transmission.

Our simulations of the sound-speed field in the region over a 24-hour period are illustrated on Figure 7, for the day on which the two acoustic Events were measured at sea. Shown is the sound-speed variability at 30 m depth (in the upper layers of the main thermocline), every 3 hours from 00:00Z Sep. 8 to 00:00Z Sep. 9, 2008. Panel (a) is the total sound-speed map on 00:00Z Sep. 8 while the other 8 Panels (b)-(i) are the differences between the subsequent 3-hourly maps and this 00:00Z Sep. 8 map. Panels are ordered according to time such that: those on the main diagonal (a, e and i) are 12 hours apart from each other (close to be in phase for the semi-diurnal tidal period); those on the first off-diagonals (b and f, d and h) are 3-hours off from those on the main diagonal; and, those on the second off-diagonals (c and g) are 6-hours off from those on the main diagonal (close to be in opposition of phase for the semi-diurnal period).

The predicted sound-speed variability maps clearly show the presence of internal tides oriented along the shelfbreak over more than a 200 km extent. They propagate up-slope and our simulations predict that their wavelength is around 40 to 80 km. These maps also indicate that the shelfbreak internal tide patterns affecting our acoustic region (the white rectangle) are weaker and not aligned with the tide patterns around the tip of Taiwan. Other internal patterns are also present in the Taiwan strait. At other depths (e.g. 60 m, 90 m, not shown), variations in time reveal similar properties. Overall, we find that the amplitude of shelfbreak internal tides decays as the waves propagate up the shelf but remain significant up to about the 80 m isobath. After 24 hours (Panel i), predicted variations also show effects of mesoscale features (eddies, fronts, etc.).

Figures 8 and 9 illustrate the sound speed variability in vertical sections along and across the shelfbreak direction, respectively. The locations of the two sections and the acoustic circles of Events A and B are plotted inside the white rectangular box drawn on the maps of Figs. 5 and 7. Panels are still shown every 3 hours during Sep. 8 (UTC). Panel (a) is the total sound-speed section on 00:00Z Sep. 8 while the other 8 Panels (b)-(i) are the differences between the subsequent 3-hourly sound-speeds and this 00:00Z Sep. 8 sound-speed.

Within the section along the shelfbreak (Fig. 8), one detects the crest and trough of wave patterns: they are aligned with the section and concentrated around the main thermocline. As shown by the 3-hourly difference fields (Panels b-i), the patterns are clearly depth-dependent (baroclinic) and of tidal period (e.g. see the negative and positive anomalies on the upper and lower first-diagonals of Fig. 8, respectively). This confirms the internal tide pattern. This signal is not small, the largest amplitudes are around 4 m/s. The vertical extent is from the bottom of the mixed layer (20 m below the ocean free surface) to about 10 m above the seafloor. The isotherms in the thermocline oscillate up and down with an amplitude of about 10-to-20 m (note that vertical oscillations of different isotherms are not exactly in phase as indicated by the baroclinic behavior).

Within the section across the shelfbreak (Fig. 9), our simulations show the train of wave patterns moving up the slope and shelf, across the shelfbreak. Again, the diagonal Panels are close to be in phase, while the most (second) off-diagonal Panels are close to be in opposition of phase with these diagonal Panels for the semi-diurnal period. The internal tide wavelength at this location and time is found to be within 40 to 60 km. The largest amplitudes of the waves in this section are around 4-5 m/s.

The internal tide variability that our simulations revealed (Figs. 8-9) was found to have significant impacts on our simulated broadband sound transmission loss in the acoustic region. These results are illustrated now. Specifically, the variations in time of our Nx2D TL simulations of Events A and B are shown in Fig. 10 again for the day (Sep. 8th, 2008) when the two OMAS runs occurred at sea. The nine different times still refer to 3-hour intervals. Panel (a) is the total broadband TL on 00:00 Sep. 8 (from 65 to 105 dB, w.r.t. a 1 m source). The other 8 Panels (b)-(i) are the differences between the subsequent 3-hourly TLs and this 00:00 Sep. 8 TL. Note that the scale for these latter differences is -10 dB to 10 dB.

Concentrating first on the shelf (Event A, blue curves), we predict relatively isotropic broadband TL variations (much more isotropic than for Event B, red curves): in other words, thermocline motions due to internal tides lead to TL variations on the shelf that are more uniform with bearing angles than they are across the shelfbreak (Event B). This is because the 6 km range of OMAS transmissions are smaller than half-a-wavelength of the internal tides (see Figs. 8 and 9). Hence, for the relatively flat shelf bathymetry, the oscillating depth of the thermocline governs the TL over 6 km. On the shelf, the anisotropy of our predicted TL over 6 km range arises because of the recurring slopes of the thermocline: see the similarity between the differences of the first lower-diagonal (Panels d and h), first upper-diagonal (Panels b and f) and second off-diagonal (Panels c and g). Note also that differences are close to zero on the main diagonal (Panels e and i: on bearing-average, -0.5 and 0.9dB, respectively). On bearing-average, the differences are largest for Panels d and h: 3.1 and 4.6dB, respectively. TL variability and sound-speed variability are not exactly in phase, in part due to the nonlinear coupling and to the 4D processes.

Over the shelfbreak (Event B, red curves), the differences between TL curves at different times are anisotropic and rapidly variable with bearing angles. At sea, it would thus be harder to distinguish coherent internal tide effects above the shelbreak. This is because the steep and complex bathymetry amplifies the internal tide oscillations into intricate bearing-dependent patterns: bottom bounces at slightly different locations actually occur at very different depths and slope angles, leading to very different transmissions. This leads to standard deviations that are larger over the shelfbreak (Event B) than over the shelf (Event A), e.g. 3.29 dB vs. 2.21 dB. However, the bearing-averaged differences are much smaller over the shelfbreak than over the shelf, as shown above. Over the shelbreak, the largest bearing-averaged differences are only -1.4 dB and 1.4 dB, for Panels (c) and (i), respectively, while on the shelf, they reach 4.6 dB for Panel (h). Our simulation results are overall in accord with observations of [22] for the South

China Sea and canonical simulations of [52], even though amplitudes are different.

Finally, one of our main results is not affected by these TL variations (Panels b-i) due to internal tides: the mean TL over the shelfbreak (Event B) is much higher between 120 and 260 degrees than the mean TL over the shelf (Event A), regardless of the internal tide properties (phase, etc). This confirms that the steep bathymetry (and not the internal tides) explains the lack of transmissions within these angles at the location and time of this shelfbreak Event B.

To show detailed effects of internal tides on the TL, full vertical sections are plotted on Figure 11. They correspond to the 0^o due north section in Fig. 10. Specifically, they are: a) and b) sound speed sections at 12:00 and 21:00 on Sep. 8th; c) difference between these two sections (9 h apart); d) and e) full field TL sections for these two times; and f), same TL estimates, but at a receiver depth of 61 meter. As seen from Panels (a-c), after nine hours, the thermocline is up by more than 10 m (note Panel c is close to be a zoom in Fig. 9d, around 120 m depth). The vertical motion of the thermocline modifies the sound-speed interface structure. As seen on Panels (d-e), this increases the width of the TL convergence zone from 1.6 km to 2 km and causes more than 10 dB variation in TL at 61 m and at 6 km range, as shown in Fig. 11(f).

On Figure 12, we show, for both Events A and B, our predicted bearing-averaged TL as a function of time during Sep. 8th (UTC). Interestingly, we find that the TL around the times of Event A (12 UTC) and, to a lesser extent, Event B (15 UTC), are within an internal tide period corresponding to higher loss, see also Fig. 10. For Event A, TL variations are due mostly to thermocline oscillations driven by internal tides and amplitudes are large, reaching 5 dB. This is significant because our TL is a broadband estimate computed by range and depth averaging (see start of Sect. III). For the single frequency TL (continuous wave - cw, computed prior to averaging), we find that these variations have amplitudes of 20 dB. The averaging reduces the amplitudes, but they are still 5 dB. In conclusion, effects of internal tides on the shelf correspond to the largest TL sensitivity that we have found among all factors studied above, almost in par with those due to very different seabed properties (see Fig. 3).

IV. Summary and Conclusions

This study was motivated by the striking difference in acoustic transmission data collected on the shelf and shelf break in the north-eastern Taiwan region within the context of the Quantifying, Predicting and Exploiting (QPE) uncertainty Pilot Experiment [24]. On the shelf, the mean acoustic transmission from a sound source moving for 6 hours along a circular track showed

little TL variation with respect to bearing angles. The largest variations there were increased loss along the northeastern direction but with small amplitudes. However, on the shelfbreak, the data for the same type of circular tracks showed no transmission when the moving source was in the deeper waters [53]. In this study, we explained, quantified, and modeled the dynamical causes of these observations. To do so, coupled oceanographic(4D)-acoustic(Nx2D) field estimation with ocean data assimilation was employed and, for the first time, compared to the observed acoustic data available. Predictive skill, uncertainties and variability in time and space were all quantified. Specifically, we studied the sensitivity of our results to uncertainties in a varied set of factors, including geo-acoustic parameters, bottom layer thickness, bathymetry and initial transport conditions in the region. We also quantified spatial and temporal effects of internal tide forcing on the the sound speed field and acoustic transmission field, both on the shelf and over the shelfbreak.

From our coupled simulations, we revealed that there were about 20 dB higher transmission losses in Event B when the sound source was in the deep water region on the shelfbreak. We showed that this dramatic increase in transmission loss is due to the deeper and complex bathymetry: our uncertainty and sensitivity studies ruled out all other factors. This is because when the sound source moved to the steep shelfbreak region with up-slope transmission, the sound propagated down at depth trapping much energy into the bottom and resulting in a TL much higher than the TL in the reverse direction with down-slope propagation over the shallower shelf.

Secondly, we investigated uncertainties in geo-acoustic parameters in both the shelf and shelfbreak acoustic simulations. We found that the sediment layer's properties led to larger but isotropic variations on the shelf (Event A) and smaller but more anisotropic variations over the shelfbreak (Event B). We also showed that our hybrid depth-dependent geo-acoustic model for the shelfbreak and sand model for the shelf better agreed with the observations than other models. Our investigations on the thickness of sediments showed that it had some limited effects (up to about 2 dB), but only on the up-slope transmissions on both Events A and B.

By comparing different sources and resolutions of accurate bathymetric data sets, we derived a statistical model of bathymetric uncertainties. Our resulting sensitivity studies on these uncertainties revealed that TL uncertainties (up to 1 dB std) were proportional to the 1 to 4% bathymetric uncertainties but that the mean TL curves did not change their shape as a function of bearing angles.

Our coupled oceanographic-acoustic modeling studies uncovered a surprising result: initial transport conditions in the Taiwan Strait can affect acoustic transmissions downstream more than 100 km away. We found that it affected the sheflbreak region (1 db std, up to 5db) more than the shelf region (0.5db std, up to 3dB). This is because the shelfbreak ocean dynamics is more sensitive to this transport than the shelf dynamics.

Using our data-assimilative ocean-acoustic full field modeling approach, we also described and studied internal tide patterns over the shelf and slope region north of Taiwan and quantified their effects on transmission loss in the acoustic region. The wave patterns revealed were clearly depth-dependent (baroclinic) and close to tidal period, affecting the whole thermocline and extending over more than 200 km on the shelf. One type of waves found were shelfbreak internal tides propagating up-slope with wavelengths around 40 to 80 km. Isotherms were simulated to oscillate up and down with amplitudes of 10-to-20 m. We discovered that these variations had significant effects on the transmission losses over 5-6 km range: on the shelf, variations of broadband TL estimates were more isotropic and relatively large (up to 5 dB) than on the shelfbreak where variations varied rapidly with bearing angles due to the steeper and more complex bathymetry. Overall, internal tides on the shelf led to the largest TL sensitivity that we simulated. For ranges of O(1-10 km), this is a signal that can be exploited.

There are several possible future research activities linked to our results. For example, we have not discussed the effects of the drifts of the OMAS sound source and of the sonobuoy receiver during the experiment since these drifts were mostly accounted for in the processed data and in our simulations set-up. For the up-slope transmissions, we also did not discuss back scattering effects that could arise due to possibly large-rock formations and volcanic effects over the shelfbreak. The azimuth angle coupling of 3D sound propagation would also affect our TL estimates, especially further near the Canyon regions. Our coupled results helped prepare for the QPE intensive observation period in the region. In general, we expect that they will be useful for diverse applications, including determining optimum sampling plans, exploiting features and improving 4D coupled acoustic-ocean data assimilation and predictions.

ACKNOWLEDGMENT

We thank P.J. Haley, W.G. Leslie and O.G. Logutov for their close collaborations. We thank P. Abbot, C. Emerson and the OASIS team for the OMAS data. We are grateful to K. Heaney, C. Holland and C.-F. Chen for discussions on seabed properties. We acknowledge J. Sen and B. Calder for their bathymetry data. We are grateful to the whole QPE team for fruitful efforts and discussions, especially G. Gawarkiewicz, T. Duda, C.-S. Chiu, B. Cornuelle, J.

Lynch, Y.-T. Lin, P. Niiler, L. Centurioni, C. Lee, R.-C. Lien, T. Sanford and H. Graber as well as the QPE team members mentioned above. We thank the US and Taiwanese research vessel crews for their work and critical data they provided. Finally, we thank D. Marble (ONR) and John Cook (NRL-Monterey) and Daniel Geiszler (SAIC) for the COAMPS and NOGAPS atmospheric products. We are grateful to the Office of Naval Research for supporting our coupled ocean-acoustic research.

REFERENCES

[1] P. Abbot and I. Dyer, "Sonar performance predictions based on environmental variability," in *Acoustic Variability*, N. Pace and F. Jensen, Eds. SACLANTCEN. Kluwer Academic Press, 2002, pp. 611–618.

[2] P. Abbot, I. Dyer, and C. Emerson, "Acoustic propagation uncertainty in the shallow east china sea." *IEEE J. Oceanic Eng.*, vol. 31, pp. 368–383, 2006.

[3] J. F. Lynch, G. G. Gawarkiewicz, C.-S. Chiu, R. Pickart, J. H. Miller, K. B. Smith, A. R. Robinson, K. Brink, R. Beardsley, B. Sperry, and G. Potty, "Shelfbreak primer an integrated acoustic and oceanographic field study in the mid-atlantic bight." in *Shallow-Water Acoustics*, R. Zhang and J. Zhou, Eds. China Ocean Press, 1997, pp. 205–212.

[4] P. F. J. Lermusiaux and C. S. Chiu, "Four-dimensional data assimilation for coupled physical-acoustical fields," in *Acoustic Variability*, N. Pace and F. Jensen, Eds. SACLANTCEN. Kluwer Academic Press, 2002, pp. 417–424.

[5] A. R. Robinson and P. F. J. Lermusiaux, "Prediction systems with data assimilation for coupled ocean science and ocean acoustics," in *Proceedings of the Sixth International Conference on Theoretical and Computational Acoustics*, et al. A. Tolstoy, Ed. World Scientific Publishing, 2004, pp. 325–342.

[6] G. Gawarkiewicz, F. Bahr, K. Brink, R. Beardsley, M. Caruso, J. Lynch, and C.-S. Chiu, "A large-amplitude meander of the shelfbreak front in the middle atlantic bight: Observations from the shelfbreak primer experiment." *J. Geophys. Res.*, vol. 109, 2004.

[7] P. F. J. Lermusiaux, C.-S. Chiu, and A. R. Robinson, "Modeling uncertainties in the prediction of the acoustic wavefield in a shelfbreak environment," in *Proceedings of the 5th International conference on theoretical and computational acoustics, May 21-25*, Q. L. E.-C. Shang and T. Gao, Eds. World Scientific Publishing Co., 2001, pp. 191–200.

[8] S. Finette, "Embedding uncertainty into ocean acoustic propagation models." *J. Acoust. Soc. Am.*, vol. 117, no. 3, pp. 997–1000, 2005.

[9] D. Wang, P. F. J. Lermusiaux, P. J. Haley, D. Eickstedt, W. G. Leslie, and H. Schmidt, "Acoustically focused adaptive sampling and on-board routing for marine rapid environmental assessment," *J. Marine Systems*, vol. 78, no. Supplement 1, pp. S393–S407, 2009.

[10] J. Xu, P. F. J. Lermusiaux, P. J. Haley, W. G. Leslie, and O. G. Logutov, "Spatial and temporal variations in acoustic propagation during the plusnet07 exercise in Dabob Bay," in *Proceedings of Meetings on Acoustics (POMA),155th Meeting Acoustical Society of America*, vol. 4, 2008, pp. 175–187.

[11] F. A. Lam, P. J. Haley, J. Janmaat, P. F. J. Lermusiaux, W. G. Leslie, M. W. Schouten, L. A. Raa, and M. Rixen, "At-sea real-time coupled four-dimensional oceanographic and acoustic forecasts during battlespace preparation 2007," *J. Marine Systems*, 2009.

[12] M. Rixen, J.-C. L. Gaca, J.-P. Hermand, G. Peggion, and E. Ferreira-Coelho, "Super-ensemble forecasts and resulting acoustic sensitivities in shallow waters," *J. Marine Systems*, vol. 78, no. Supplement 1, pp. S290–S305, 2009.

[13] O. Carriére, J.-P. Hermand, J.-C. L. Gac, and M. Rixen, "Full-field tomography and kalman tracking of the range-dependent sound speed field in a coastal water environment," *J. Marine Systems*, vol. 78, no. Supplement 1, pp. S382–S392, 2009.

[14] N. E. Martins and S. M. Jesus, "Bayesian acoustic prediction assimilating oceanographic and acoustically inverted data," *J. Marine Systems*, vol. 78, no. Supplement 1, pp. S349–S358, 2009.

[15] J. Lynch, A. Newhall, B. Sperry, G. Gawarkiewicz, P. Tyack, and C.-S.Chiu, "Spatial and temporal variations in acoustic propagation characteristics at the new england shelfbreak front." *IEEE J. Oceanic Eng.*, vol. 28, pp. 129–150, 2001.

[16] P. F. J. Lermusiaux, C.-S. Chiu, G. Gawarkiewicz, P. Abbot, A. Robinson, R. Miller, P. Haley, W. Leslie, S. Majumdar, A. Pang, and F. Lekien, "Quantifying uncertainties in ocean predictions." *Oceanography, Special issue on "Advances in Computational Oceanography"*, vol. 19, no. 1, pp. 92–105, 2006.

[17] Y.-T. Lin, A. E. Newhall, T. F. Duda, P. F. J. Lermusiaux, and P. J. Haley, "Statistical merging of data sources to estimate full water-column sound speed in the new jersey shallow water 2006 experiment," *IEEE Ocean Engineering*, Submitted.

[18] P. Dahl, R. Zhang, J. Miller, L. Bartek, Z. Peng, S. Ramp, J.-X. Zhou, C.-S. Chiu, J. Lynch, J. Simmen, and R. Spindel, "Overview of results from the asian seas international acoustics experiment in the east china sea." *IEEE J. Oceanic Eng.*, vol. 29, pp. 920–928, 2004.

[19] J. Lynch, S. Ramp, C.-S. Chiu, T. Y. Tang, Y.-J. Yang, and J. Simmen, "Research highlights from the asian seas international acoustics experiment in the south china sea," *IEEE J. Oceanic Eng.*, vol. 29, pp. 1067–1074, 2004.

[20] S. Ramp, C.-S. Chiu, F. Bahr, Y. Qi, P. Dahl, J. Miller, J. Lynch, R. Zhang, and J. Zhou, "The shelf-edge frontal structure in the central east china sea and its impact on low-frequency acoustic propagation." *IEEE J. Oceanic Eng.*, vol. 29, pp. 1011–1031, 2004.

[21] T. Duda, J. Lynch, J. Irish, R. Beardsley, S. Ramp, C.-S. Chiu, T. Y. Tang, and Y.-J. Yang, "Internal tide and nonlinear internal wave behavior at the continental slope in the northern south china sea." *IEEE J. Oceanic Eng.*, vol. 29, pp. 1105–1130, 2004.

[22] T. F. Duda, J. F. Lynch, A. E. Newhall, L. Wu, and C.-S. Chiu, "Fluctuation of 400-hz sound intensity in the 2001 asiaex south china sea experiment," *IEEE J. Oceanic Eng.*, vol. 29, pp. 1264–1279, 2004.

[23] W. A. Kuperman and J. F. Lynch, "Shallow-water acoustics," *PHYSICS TODAY*, vol. 57, pp. 55–61, 2004.

[24] G. Gawarkiewicz, "Quantifying, predicting, exploiting uncertainty(QPE), 2008 pilot experiment; Aug 22nd - Sep. 11th, 2008 technical report." Woods Hole Oceanographic Institute, Tech. Rep. Interim report, 48pp, 2008.

[25] T. Y. Tang, Y. Hsueh, Y. J. Yang, and J. C. Ma, "Continental slope flow northeast of taiwan." *Journal OF Physical Oceanography*, vol. 29, pp. 1353–1362, 1999.

[26] P. F. J. Lermusiaux, P. J. Haley, W. G. Leslie, O. Logutov, J. Xu, and E. V. Heubel, "http://mseas.mit.edu/Sea_exercises/QPE/".

[27] C.-F. Chen and J.-J. Lin, "Three dimensional effect on acoustic transmission in taiwan's north-eastern sea,," in *Proceedings of International Shallow-Water Acoustics*. Beijing, 1997.

[28] T. F. Duda and L. Rainville, "Diurnal and semidiurnal internal tide energy flux at a continental slope in the south china sea." *J. Geophys. Res.*, vol. 113, 2008.

[29] P. J. Haley and P. F. J. Lermusiaux, "Two-way embedding schemes for multiscale primitive-equations with a free ocean surface." *Ocean Dynamics*, 2010.

[30] P. J. Haley, P. F. J. Lermusiaux, W. G. Leslie, and A. R. Robinson, "Harvard ocean prediction system (HOPS)," http://mseas.mit.edu/HOPS, Tech. Rep., 1999.

[31] P. J. Haley, P. F. J. Lermusiaux, A. R. Robinson, W. G. Leslie, O. Logutov, G. Cossarini, X. S. Liang, P. Moreno, R. S. R., J. D. Doyle, J. Bellingham, F. Chavez, and S. Johnston, "Forecasting and reanalysis in the monterey bay/california current region for the autonomous ocean sampling network-ii experiment." *Special issue on AOSN-II, Deep Sea Research, Part II*, 2009, iSSN 0967-0645, DOI: 10.1016/j.dsr2.2008.08.010.

[32] A. Argawal and P. F. J. Lermusiaux, "Statistical field estimation for complex coastal regions and archipelagos." *Ocean Modeling*, 2010.

[33] P. F. J. Lermusiaux, "Estimation and study of mesoscale variability in the strait of sicily," *Dynamics of Atmospheres and Oceans*, vol. 29, pp. 255–303, 1999.

[34] P. F. J. Lermusiaux, A. R. Robinson, P. J. Haley, and W. G. Leslie, "Filtering and smoothing via error subspace statistical estimation," in *Advanced interdisciplinary data assimilation*, The OCEANS 2002 MTS/IEEE. Holland Publications, 2002, pp. 795–802.

[35] P. F. J. Lermusiaux, "Uncertainty estimation and prediction for interdisciplinary ocean dynamics," *Journal of Computational Physics, Special issue of on "Uncertainty Quantification". J. Glimm and G. Karniadakis, Eds.*, pp. 176–199, 2006.

[36] ——, "Adaptive sampling, adaptive data assimilation and adaptive modeling." *Physica D., Special issue on "Mathematical Issues and Challenges in Data Assimilation for Geophysical Systems: Interdisciplinary Perspectives", Christopher K.R.T. Jones and Kayo Ide, Eds.*, vol. 230, pp. 172–196, 2007.

[37] T. P. Sapsis and P. F. J. Lermusiaux, "Dynamically orthogonal field equations for continuous stochastic dynamical systems." *Physica D.*, vol. 238, pp. 2347–2360, 2009.

[38] R. C. Tian, P. F. J. Lermusiaux, J. J. McCarthy, and A. R. Robinson, "A generalized prognostic model of marine biogeochemical-ecosystem dynamics: Structure, parameterization and adaptive modeling," Harvard Reports in Physical/Interdisciplinary Ocean Science, Tech. Rep. No.67, 2008.

[39] O. G. Logutov and P. F. J. Lermusiaux, "Inverse barotropic tidal estimation for regional ocean applications," *Ocean Modeling*, vol. 25, pp. 17–34, 2008.

[40] M. S. Lozier, W. B. Owens, and R. G. Curry, "The climatology of the north atlantic." *Progress in Oceanography*, vol. 36, pp. 1–44, 1995.

[41] S. Jan, 2008, Personal communication.

[42] P. F. J. Lermusiaux, "Error subspace data assimilation methods for ocean field estimation: theory, validation and applications," Ph.D. Thesis, Harvard University, Tech. Rep., 1997.

[43] A. L. Perkins, L. F. Smedstad, D. W. Blake, G. W. Heburn, and A. J. Wallcraft, "A new nested boundary condition for a primitive equation ocean model." *J. Geophys. Res.*, vol. 102, no. C2, pp. 3483–3500, 1997.

[44] P. F. J. Lermusiaux, P. J. Haley, W. G. Leslie, O. Logutov, J. Xu, and E. V. Heubel, "http: //mseas.mit.edu /Sea_exercises/QPE/Maps/Sep10/Skill/".

[45] B. Calder, 2009, Personal communication.

[46] C. M. Ferla, M. B. Porter, and F. B. Jensen, *C-SNAP: Coupled SACLANTCEN normal mode propagation loss model*. SACLANTCEN document SM-274, 1993.

[47] C. H. Harrison and J. A. Harrison, "A simple relationship between frequency and range averages for broadband sonar." *J. Acoust. Soc. Am.*, vol. 97, no. 2, pp. 1314–1317, 1995.

[48] E. L. Hamilton, "Geoacoustic modeling of the sea floor." *J. Acoust. Soc. Am.*, vol. 68, no. 5, pp. 1313–1340, 1980.

[49] F. B. Jensen, W. A. Kuperman, M. B. Porter, and H. Schmidt, Eds., *Computational Ocean Acoustics*, ser. AIP series in modern acoustics and signal processing, P36-38. AIP Press: Springer, 2000.

[50] K. Heaney, "Sensitivity analysis for QPE pilot study – draft 1," OASIS Inc., Tech. Rep. 24pp, 2008.

[51] S. Jan and S.-Y. Chao, "Seasonal variation of volume transport in the major inflow region of the taiwan strait: the penghu channel." *Deep-Sea Research II*, vol. 50, pp. 1117–1126, 2003.

[52] S. Finette, R. Oba, C. Shen, and T. Evans, "Acoustic propagation under tidally driven, stratified flow." *J. Acoust. Soc. Am.*, vol. 121, no. 5, pp. 2575–2590, 2007.

[53] P. Abbot and C. Emerson, 2009, Personal communication.

Pierre F.J. Lermusiaux received B.&M. in Mech. Eng. degrees (highest honors and Jurybs congratulations) from Liege University, Liege, Belgium, in 1992 and the S.M. and Ph.D. degrees in engineering sciences from Harvard University, Cambridge, MA, in 1993 and 1997. Currently, he is an Associate Professor of Mechanical Engineering, Massachusetts Institute of Technology, Cambridge. His current research interests include physical and interdisciplinary ocean dynamics, from submesoscales to interannual scales. They involve physical-biogeochemical-acoustical ocean modeling, optimal estimation and data assimilation, uncertainty and error modeling, and the optimization of observing systems. Dr. Lermusiaux has held Fulbright Foundation Fellowships, was awarded the Wallace Prize at Harvard in 1993, presented the Ogilvie Young Investigator Lecture in Ocean Engineering at MIT in 1998 and was awarded a Doherty Associate Professorship in Ocean Utilization by MIT in 2009. He is a member of the Association of Engineers of Liege University, Friends of the University of Liege, Royal Meteorological Society, American Geophysical Union, Oceanography Society, American Association for the Advancement of Science and Society for Industrial and Applied Mathematics.

Jinshan Xu received the B.A. degree in electrical engineering and the Sc.M. in physical oceanography from University of Qingdao, Qingdao, China, in 1994 and 1999, and the Ph.D. degrees in mechanical and oceanographic engineering from Massachusetts Institute of Technology/Woods Hole Oceanographic Institute Joint Program in Oceanography, in September 2007. Currently, he is a Postdoctoral Research Associate in the Mechanical Engineering Department, Massachusetts Institute of Technology, Cambridge. His research interests are in the areas of underwater acoustic propagation modeling and signal processing, wave propagation through random media. Dr. Xu is a member of the Acoustical Society of America.

LIST OF FIGURES

LIST OF TABLES

	Cp (m/s)	Rho (g/cm^3)	Attn (dB/λ)
Sand	1562	1.9	0.90
	1550$\sim$1650		0.25$\sim$ 1.0
Muddy-Sand	1549	1.488	1.15
	1540$\sim$1575		0.4 $\sim$1.25
Clay	1460	1.421	0.1
			0.03 $\sim$ 0.2
Basement	1800	2.0	0.5

TABLE I

SEABED PROPERTIES OF THREE DIFFERENT SEDIMENT MODELS AND OF THE BASEMENT. FOR EACH SEDIMENT MODEL: THE FIRST LINE GIVES THE OPTIMUM VALUES WE OBTAINED, THE SECOND LINE INDICATES THE DEVIATION RANGES OF THE PARAMETER VALUES THAT WE TESTED ON. OVERALL, MORE THAN THIRTY SEDIMENT MODEL VALUES WERE COMPARED.

Shallow water	$Z < 140$ m	Sand
Shelf Break	$140 < Z < 210$ m	Muddy-sand
Continental Slope	$Z > 210$ m	Clay

TABLE II

DEPTH-DEPENDENT SEDIMENT MODEL, RESULTING OF A BEST-FIT OF OUR COUPLED OCEAN-ACOUSTIC MODELS TO TL OBSERVATIONS. NOTE THAT MORE THAN 10 SETS OF TWO TRANSITION DEPTHS WERE TESTED, ONLY THE BEST-FIT IS REPORTED HERE.

V. FIGURES

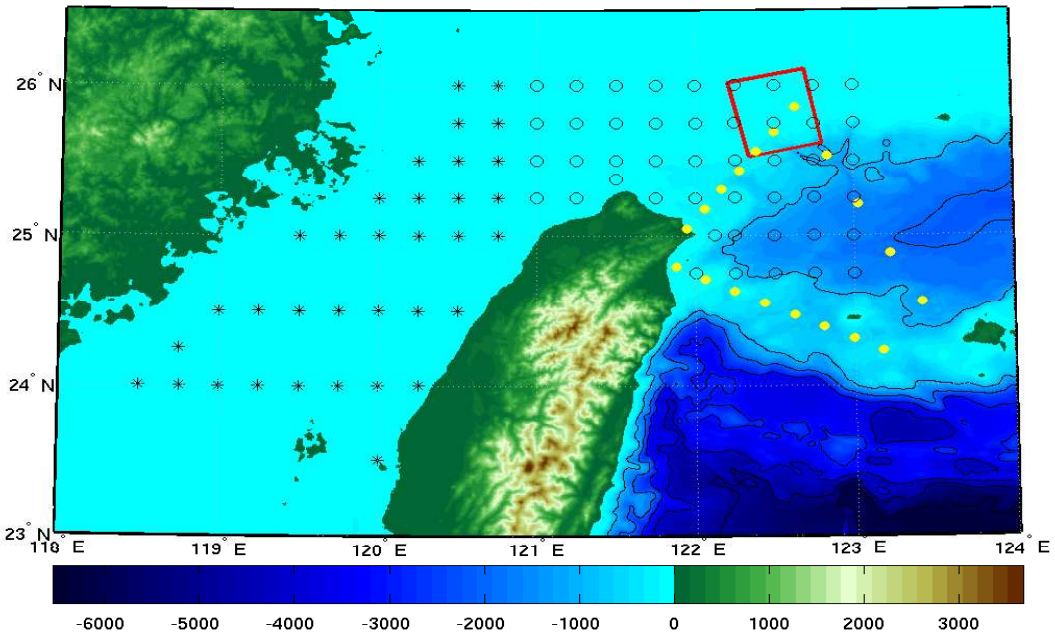

(a)

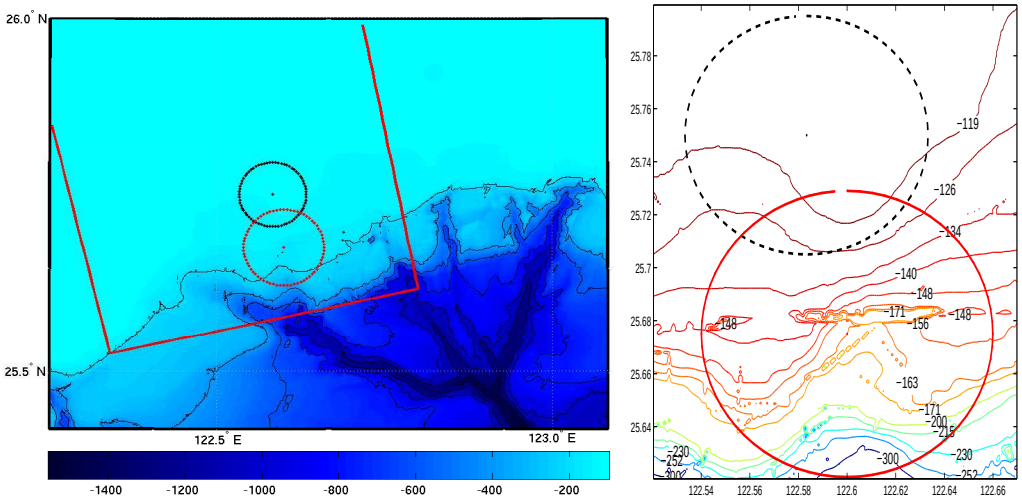

(b) (c)

Fig. 1. a) QPE Pilot Experiment - CTD stations and Main Study Area. The intensive acoustic region is identified by the solid box. The solid dots are CTD stations for the OR1 Leg 1,2 cruises; stars for the OR2 cruise, and circles for the OR3 cruise. b) Bathymetry (m) of the Acoustic Experiment region overlaid with the two planned tracks of the OASIS Mobile Acoustic Source (OMAS) circle runs, refereed to as Events A and B. c) Bathymetry (m) at locations of Events A and B.

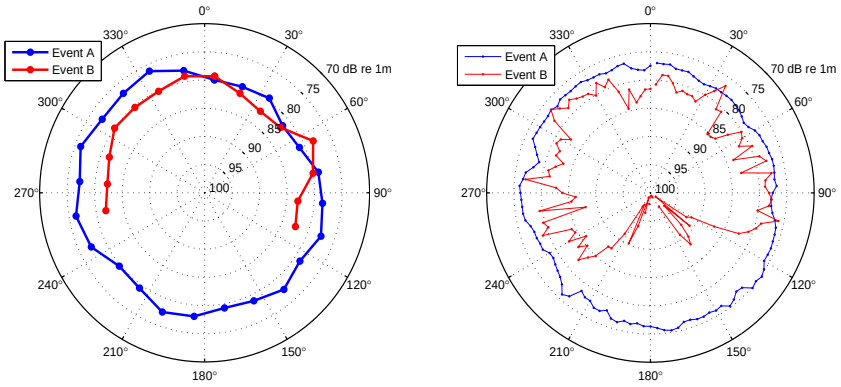

(a) (b)

Fig. 2. a) Measured mean TL of Events A (blue, with observed bearing-averaged $\sigma = 1.8$ dB) and B (red, with $\sigma = 2.4$ dB) [53]. b) Coupled ocean(4D)-acoustics(Nx2D) simulations of the mean TL of Event A (blue, with bearing-averaged $\sigma = 1.23$ dB) at 12:00 UTC, September 8, 2008, and Event B (red, with $\sigma = 2.33$ dB in the bearing angle ranges: ≥ 260 degree or ≤ 110 degree; $\sigma = 7.87$ dB for whole circle) at 15:00 UTC, September 8, 2008.

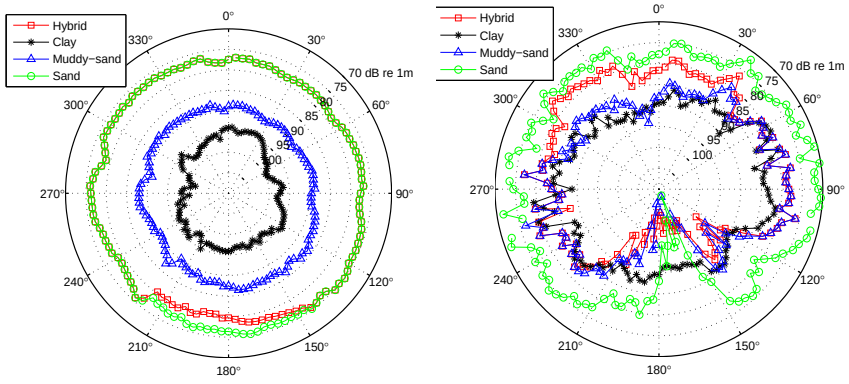

(a) (b)

Fig. 3. Nx2D TL simulations of Events A and B, illustrating effects of different sediments models (and keeping all other factors constant: in particular, the sediment sickness is set to 20 m). The four different sediments discussed here were: depth-dependent (hybrid) model with variable sediments, sand, muddy-sand, and silty-clay. With these sediment variations, one obtains a standard deviation for Event A of $\overline{\sigma_{TL_{sediment}}(\theta)} = 9.55$ dB and for Event B of $\overline{\sigma_{TL_{sediment}}(\theta)} = 5.81$ dB. The ocean fields are those of 12:00 pm, Sep. 8, 2008 (UTC).

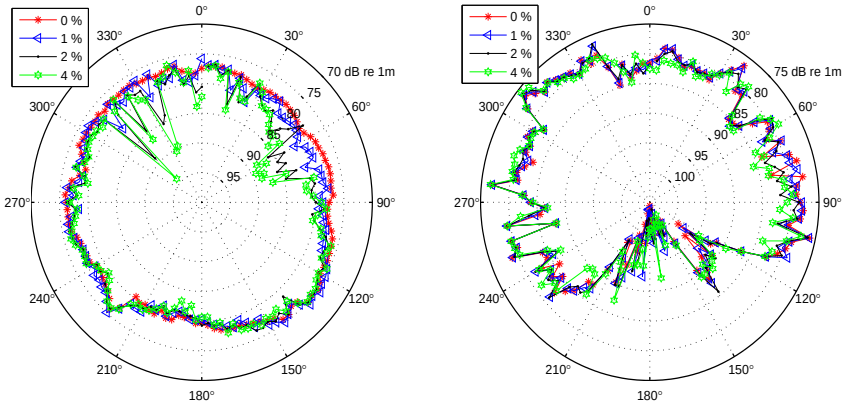

(a) (b)

Fig. 4. Nx2D TL simulations of Event A ($\overline{\sigma_{TL_{bathymetry}}(\theta)} = 1.25$ dB) and Event B ($\overline{\sigma_{TL_{bathymetry}}(\theta)} = 1.02$ dB) with different percentages of random perturbation on the 100m-resolution bathymetry data. The normally distributed random noise was added on the bathymetry with a variance proportional to the slope and to the local depth. The ocean fields are those of 12:00 pm, Sep. 8, 2008 (UTC).

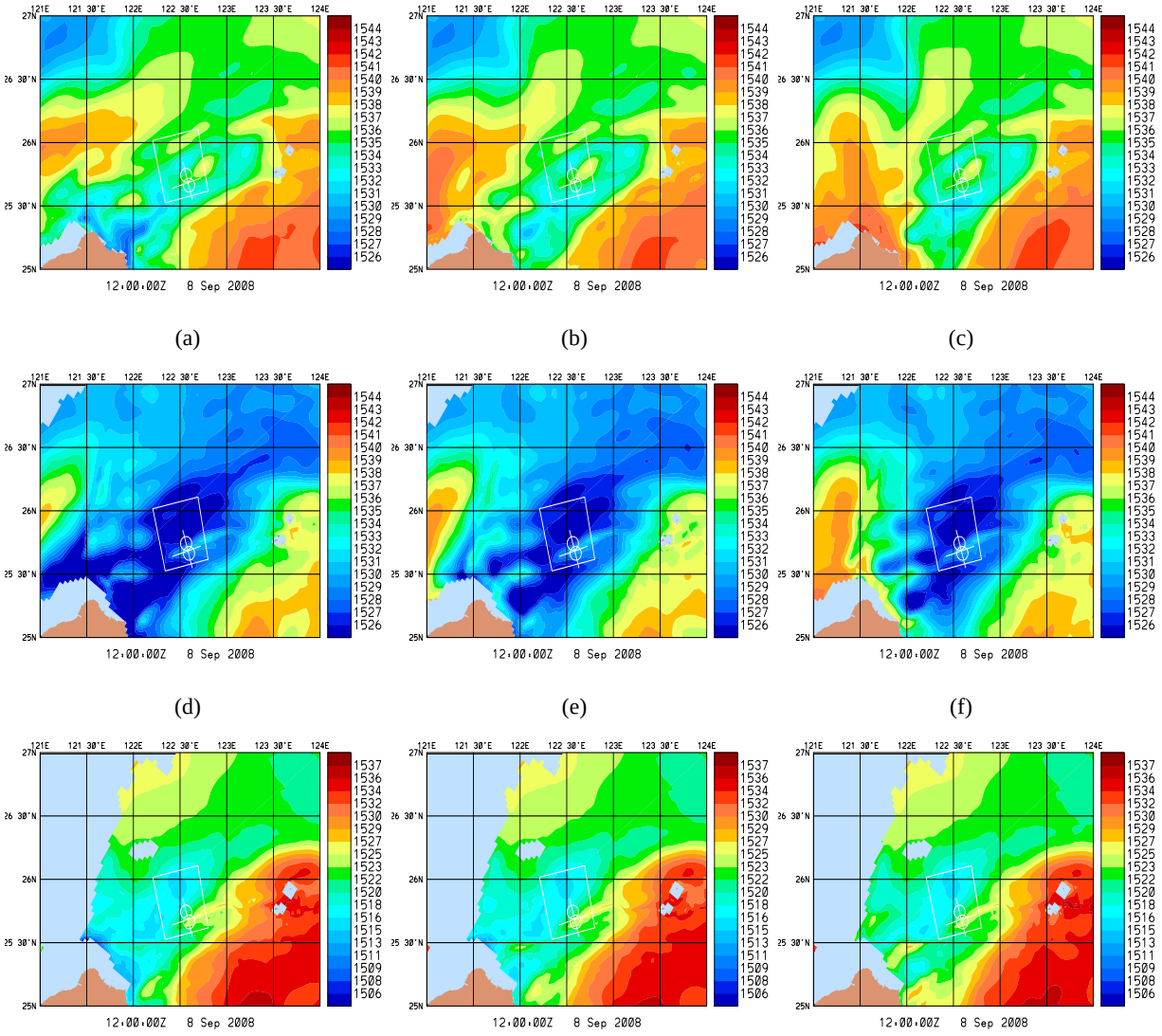

Fig. 5. Predicted ocean sound speed field at 30 m (a b c), 60 m (d e f), and 90 m (g h i) depth at 12:00 pm, Sep. 8, 2008 (UTC), which is the day when Events A and B occurred at sea. Each column corresponds to a different initial condition for the vertically-averaged transport in the Taiwan Strait: First column - 1 Sv S; Second column - 0 Sv; Third column - 1 Sv N.

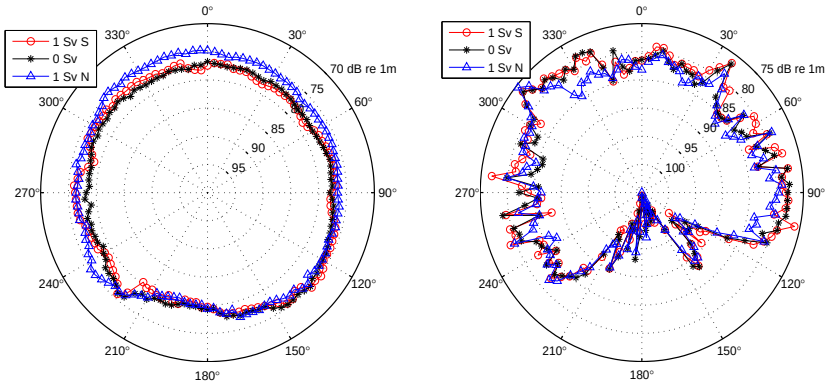

(a) (b)

Fig. 6. Nx2D TL simulations of Event A ($\overline{\sigma_{TL_{initial}}(\theta)} = 0.58$ dB) and Event B ($\overline{\sigma_{TL_{initial}}(\theta)} = 1.21$ dB) at 12:00 pm, Sep. 8, 2008 (UTC) corresponding to different ocean field predictions (transport conditions between Taiwan and mainland China initialized at ± 1 or 0 Sv, as illustrated on Fig. 5) used as inputs for the background sound speed field.

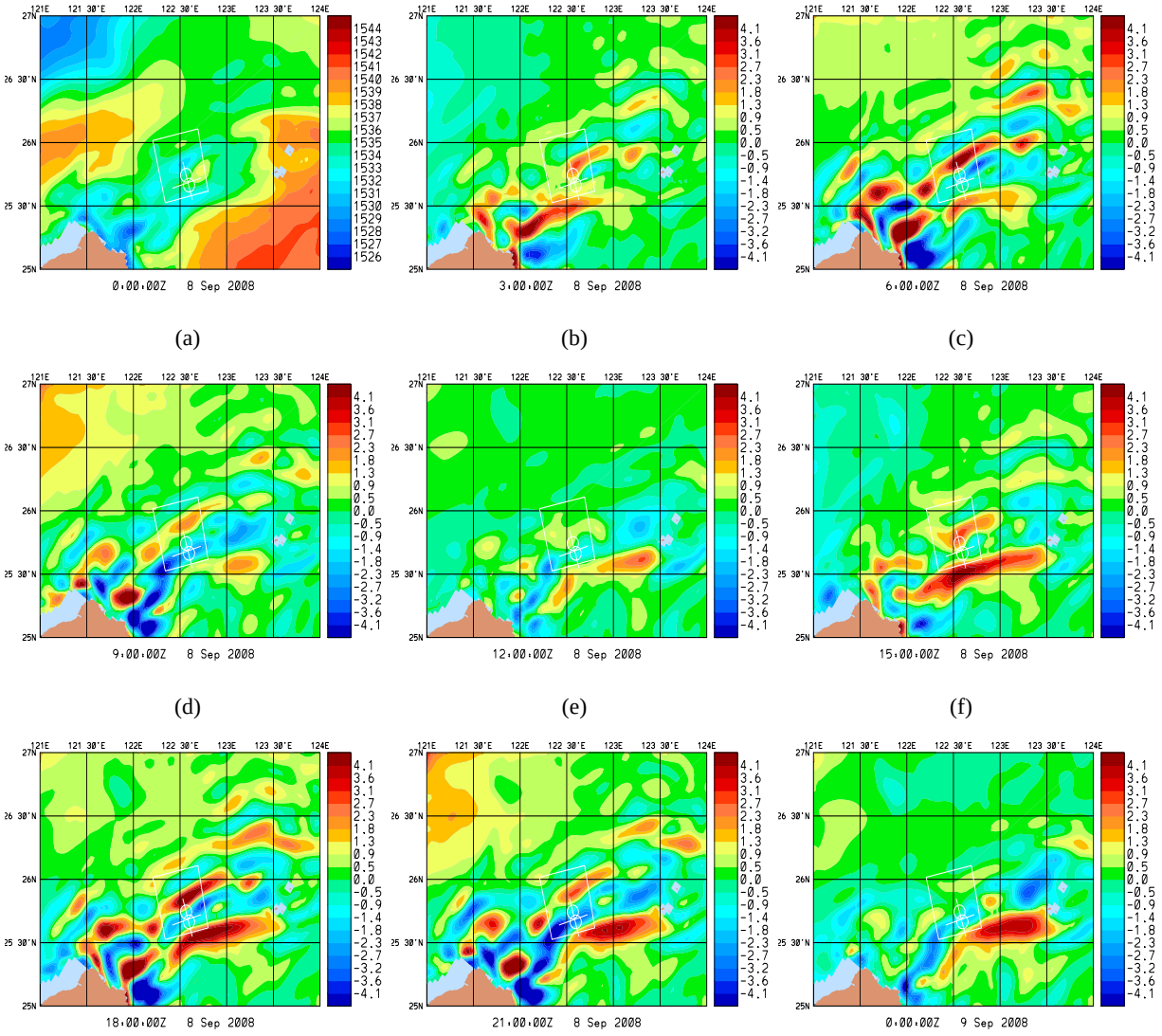

Fig. 7. Predicted sound-speed variability maps at a depth of 30 meter: (a)-(i) correspond to the times from 00:00 Sep 8 to 00:00 Sep 9, 2008 (UTC) with three hours interval. Panel (a) is the total sound-speed on 00:00 Sep 8 while Panels (b)-(i) are differences between the subsequent 3-hourly sound-speed fields and this 00:00 Sep 8 field.

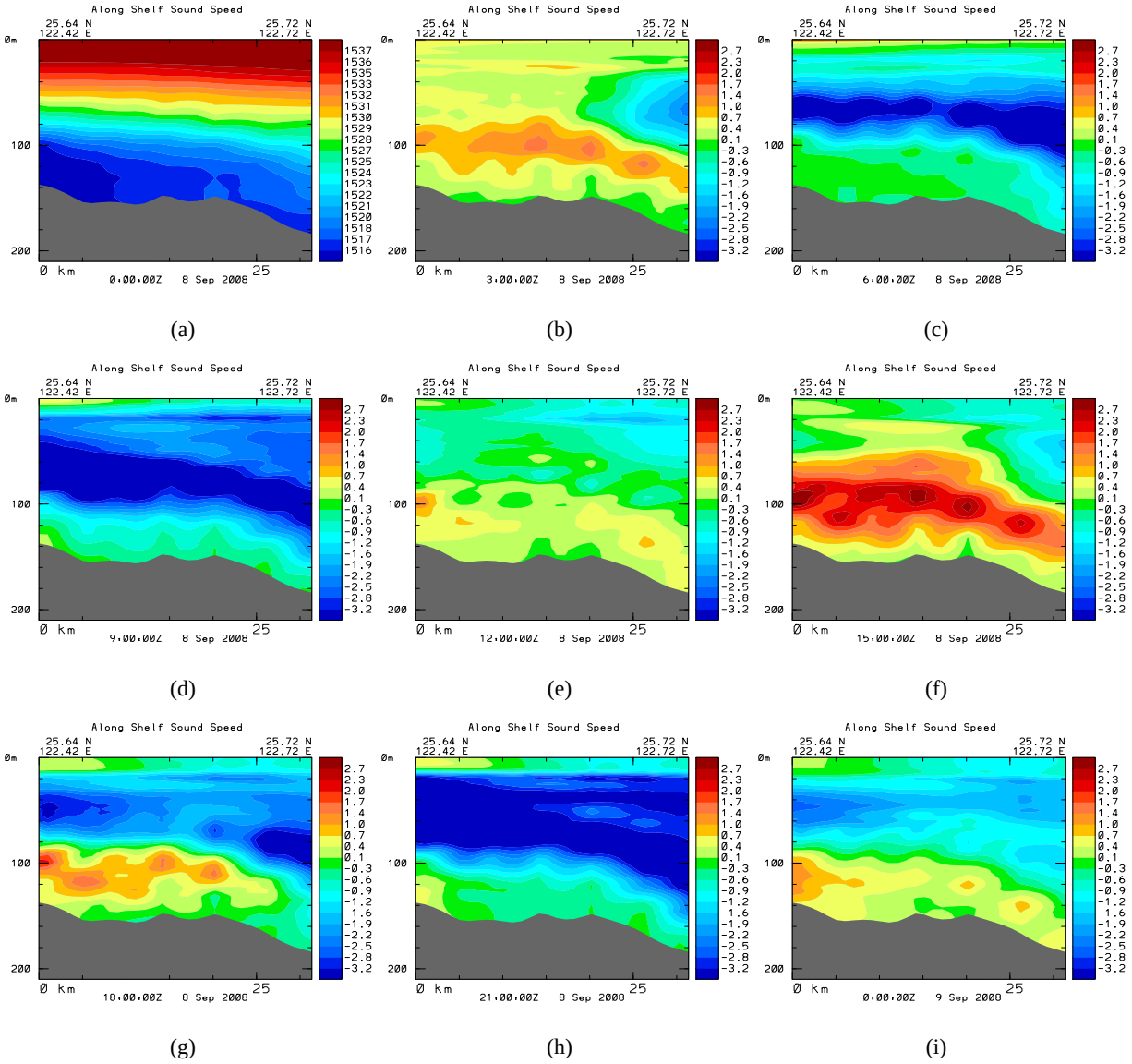

Fig. 8. Predicted sound-speed variability section, along the shelf, within the acoustic region: (a)-(i) correspond to the times from 00:00 Sep 8 to 00:00 Sep 9, 2008 (UTC) with three hours interval. Panel (a) is the total sound-speed on 00:00 Sep 8 while Panels (b)-(i) are differences between the subsequent fields and this 00:00 Sep 8 field.

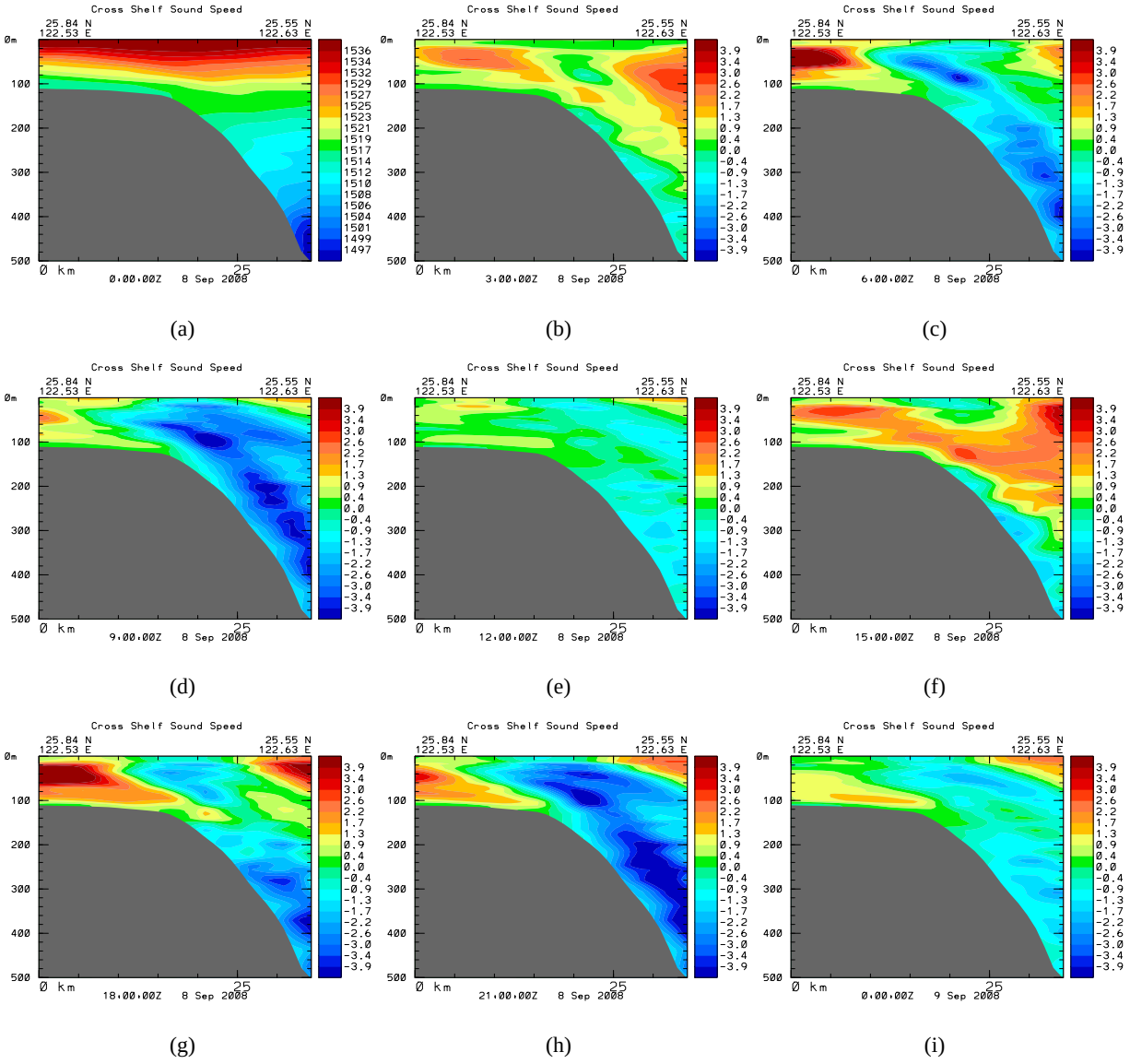

Fig. 9. As Fig. 8, but for the across-shelf section within the acoustic region.

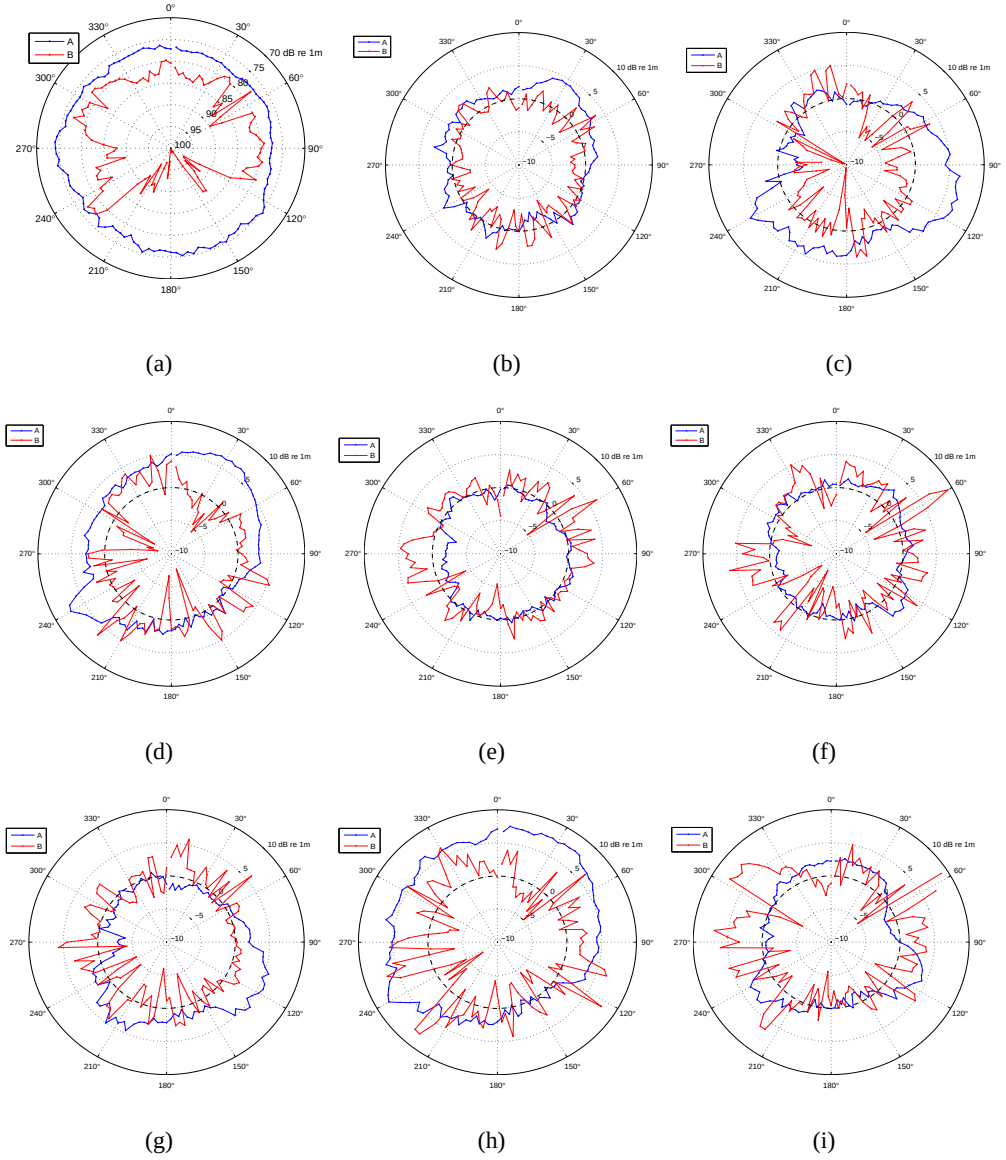

Fig. 10. Nx2D TL simulations of Event A (blue-curves, $\overline{\sigma_{TL_{tide}}(\theta)} = 2.21$ dB) and Event B (red-curves, $\overline{\sigma_{TL_{tide}}(\theta)} = 3.29$ dB, in the bearing angle ranges: $\geq$ 260 degree or $\leq$ 110 degree; $\sigma = 7.64$ dB for whole circle at different times). Panels (a)-(i) again correspond to the times from 00:00 Sep 8 to 00:00 Sep 9, 2008 (UTC) with three hours interval. This includes the period during which Events A and B actually occurred at sea. Panel (a) is the total TL on 00:00 Sep 8 while Panels (b)-(i) are differences between the subsequent TL fields and this 00:00 Sep 8 field. The TL range for these differences is from -10 dB to 10 dB: the dashed circle denotes the 0 dB.

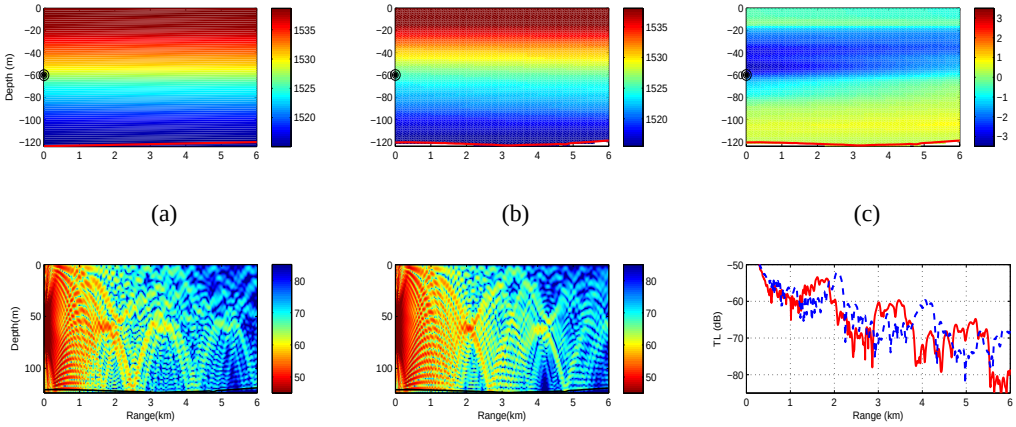

Fig. 11. Sections on Sep.8th, 2008, all times UTC: a) sound speed at 12:00; b) sound speed at 21:00; c) difference of sound speeds between a) and b); d) TL estimate at 12:00; e) TL estimate at 21:00; e) TL estimates for a receiver at 61 m, at 12:00 (red) and 21:00 (blue).

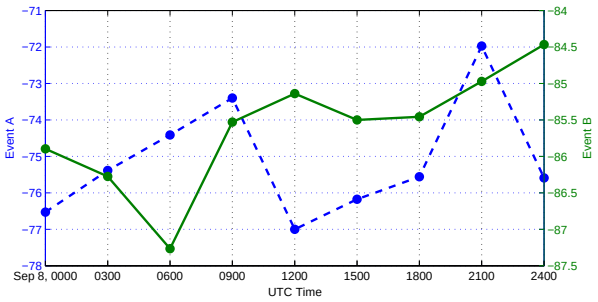

Fig. 12. Bearing-averaged TL estimates for Events A and B every three hours during Sep. 8th (UTC).